Physica A 509 (2018) 729–745

Contents lists available at ScienceDirect

Physica A

journal homepage: www.elsevier.com/locate/physa

Develop the lattice Boltzmann method to simulate the slip velocity and temperature domain of buoyancy forces of FMWCNT nanoparticles in water through a micro flow imposed to the specified heat flux

Arash Karimipour [a], Annunziata D'Orazio [b], Marjan Goodarzi [c,*]

[a] Department of Mechanical Engineering, Najafabad Branch, Islamic Azad University, Najafabad, Iran
[b] Dipartimento di Ingegneria Astronautica, Elettrica ed Energetica, Sapienza Università di Roma, Via Eudossiana 18, Roma 00184, Italy
[c] Sustainable Management of Natural Resources and Environment Research Group, Faculty of Environment and Labour Safety, Ton Duc Thang University, Ho Chi Minh City, Vietnam

HIGHLIGHTS

- Develop LBM ability to simulate effects of buoyancy forces.
- Water/FMWCNT slip velocity through a micro flow.
- Simulation of specified heat flux along microchannel by LBM.

ARTICLE INFO

Article history:
Received 22 February 2018
Received in revised form 20 May 2018
Available online xxxx

Keywords:
Lattice Boltzmann
Micro flow
Specified heat flux
Carbon nanotubes

ABSTRACT

Lattice Boltzmann method ability is improved to simulate the mixed convection of Water / FMWCNT nanofluid inside a two dimensional microchannel. The influences of gravity on hydrodynamic and thermal domains are studied while the microchannel walls are imposed by a constant thermal heat flux at three different case studies as no-gravity, $Ri = 1$ and $Ri = 10$. The flow Reynolds number is chosen as one and the liquid micro flow conditions are involved by $B = 0.005$, $B = 0.01$ and $B = 0.02$. The mass fraction of carbon nanotubes in water are selected as $\phi = 0$, $\phi = 0.1\%$ and $\phi = 0.2\%$. Double population distribution functions of "f" and "g" are used in lattice Boltzmann method. To the best of author's knowledge, there is no article concerned the way of heat flux boundary condition simulation by LBM considering the buoyancy forces effects on nanofluid slip velocity. Generate a rotational cell due to gravity in entrance region which leads to observe the negative slip velocity phenomenon can be presented as the several interesting achievements of this work.

1. Introduction

Micro devices, which are concerned fluid flow and heat transfer in micro and nano scales level (MEMS & NEMS), have different applications in nowadays industries which lead to report a large number of studies about them. It should be noticed to different specifications of macro flows in comparison with micro and nano ones. The different level of a micro and a nano flow is presented by dimensionless Kudsen number which is shown by $Kn = \lambda/D_H$ where λ represents the molecular mean

* Corresponding author.
E-mail address: marjan.goodarzi@tdt.edu.vn (M. Goodarzi).

https://doi.org/10.1016/j.physa.2018.06.031
0378-4371/

Nomenclature

B	Dimensionless liquid slip coefficient
c	Vector of velocity in microscopic scale
c_s	Sound speed in lattice scale
D_H	Microchannel hydraulic diameter
f	Hydrodynamic distribution function
FMWCNT	Functionalized multi-walled carbon nanotubes
g	Thermal distribution function
H	Microchannel height
L	Microchannel length
Kn	Knudsen number
q	Imposed heat flux, Wm^{-2}
Re	Reynolds number
$Ri = Gr/Re^2$	Richardson number
T	Dimensional temperature, k
u	Vector of velocity in macroscopic scale, ms^{-1}
(U,V)	Dimensionless velocities in macroscopic scale
U_s	Dimensionless slip velocity
(X,Y)	Coordinates in dimensionless forms

Greek symbols

$\theta = T/T_i$	Dimensionless temperature in macroscopic scale
ϕ	Mass fraction of carbon nanotubes

free pass [1–16]. For the state of $Kn < 0.001$, the flow field will be continues which means the classic Navier–Stokes equations can be used; however these equations are able to simulate the fluid flow at slip flow regime ($0.001 < Kn < 0.1$) considering the slip velocity and temperature jump boundary conditions along the solid walls. The transient and free molecular regimes are also achieved at higher values of Knudsen number as $0.1 < Kn < 10$ and $Kn > 10$ which only the particle base methods must be applied [17–27].

Various types of particle base methods have been introduced by now; among them three approaches of Direct Simulation of Monte Carlo, Molecular Dynamic and Lattice Boltzmann method (LBM) have been found more suitable at different aspects like accuracy and convergence. LBM, MD and DSMC can be used in all flow regimes; however using MD and DSMC will be much more time consuming at macro scales due to working with interactions between the molecules. A lot of works can be addressed using these approaches in micro and nano flows [28–43]. LBM uses a parallel algorithm with less complex formulation; it also shows suitable accuracy and is appropriate for the simulation of multi-phase flows. Moreover the incompressible Navier–Stokes equations can be derived from Boltzmann equation by using BGK model. In general LBM is a relatively new method to simulate a gas flow according to the collision and propagation of the fictive particles on the lattice points at each time step. The collision operator is also chosen in a way to satisfy the conservative laws in LBM-BGK model. LBM works only with density–momentum distribution function of "f" for the hydrodynamic domain in the lattice scale; then all other physical parameters like macroscopic velocity and density are estimated from it. This fact makes LBM easier than the well-known CFD methods [44–58].

Double population distribution function was developed to cover the both hydrodynamic and thermal fields in LBM. In this method, another distribution function of "g" (internal energy distribution function) was introduced. "g" could be illustrated based on "f" and represented the internal energy and temperature. This type of LBM was shown by TLBM and many works corresponded in this way at macro and micro scales [59–72].

Usual fluids like water and oils have low values of thermal conductivity which imply the conduction heat transfer mechanism can be neglected through them. Adding a little measured metal or non-metal nanoparticles like Al, Cu, Ag or Al_2O_3 to the base fluid, would increase the mixture conduction coefficient; so that both conduction and convection heat transfer mechanisms will have noticeable rolls. This mixture was called nanofluid and various types of solid nanoparticles and base fluids have been examined in this way by now. Many works can be referred to generate different kinds of nanofluids or using them at different conditions and geometries. However because of extraordinary properties of Carbon nanotubes (CNT) especially their large thermal conductivity, much attention have been paid to use CNT to generate the suitable nanofluid [73–98]. Hence it is claimed that double population distribution functions approach of LBM has not been applied to simulate the effects of gravity on slip velocity and temperature domain of a nanofluid in a micro flow; however present work intends to improve LBM performance in such mentioned cases for the first time.

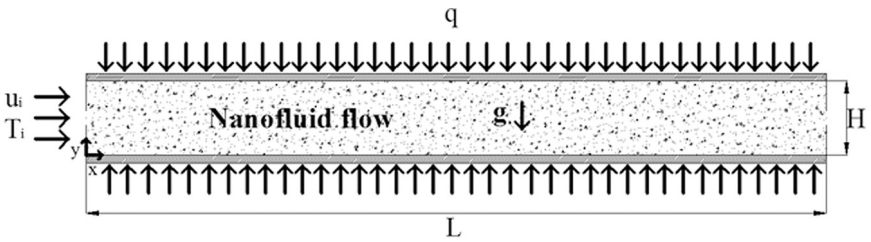

Fig. 1. The schematic of the microchannel affected by constant heat flux.

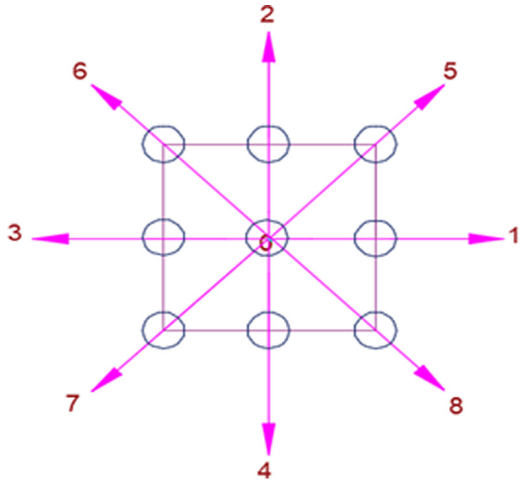

Fig. 2. The lattice of D_2Q_9.

2. Problem statement

Mixed convection of nanofluid, composed of water/FMWCNT (functionalized multi walled carbon nanotubes), in a long microchannel (L/H = 10) is simulated using TLBM-BGK for the first time as its sidewalls are affected by a heat flux of q_0''. The solution process is performed in dimensionless form. Hence there is no need to know the value of constant heat flux based on the way to define the dimensionless parameters. The influences of buoyancy forces through a nanofluid micro flow has been ignored in the most previous articles specially by using LBM. So present work will try to vanish this lack of research, besides increase LBM ability to develop its domain performance.

Using nanofluid composed of carbon nanotubes (CNT) dispersed in water through a microchannel, was reported by Nikkhah et al. [33] and also the influences of buoyancy forces of the air flow at the micro scales level were presented in Ref. [8]; these both articles would represent the physical possibility of the supposed present problem.

As shown in Fig. 1, the temperature of inlet cold nanofluid (T_i) will increase through the microchannel due to heat exchange with hot walls. Effects of buoyancy forces on slip velocity and temperature domain at different values of mass fraction of carbon nanotubes ($\phi = 0$, $\phi = 0.1\%$, $\phi = 0.2\%$) are investigated. To do this, three different case studies as no-gravity, $Ri = 1$ and $Ri = 10$ at $Re = 1$ are considered while the dimensionless liquid slip coefficient changes from B = 0.005 to B = 0.01 and B = 0.02. Double population distribution functions of "f" and "g" in thermal lattice Boltzmann method are used for the hydrodynamic and thermal domains.

3. Equations

3.1. Lattice Boltzmann Method

Boltzmann equation based on hydrodynamic and thermal distribution functions [24]:

$$\partial_t f + (\boldsymbol{c} \cdot \nabla) f = \Omega(f) \tag{1}$$

$$g = 0 \cdot 5\,(\boldsymbol{c} - \boldsymbol{u})^2 f \tag{2}$$

$$\partial_t g + (\boldsymbol{c} \cdot \nabla) g = \Omega(g) \tag{3}$$

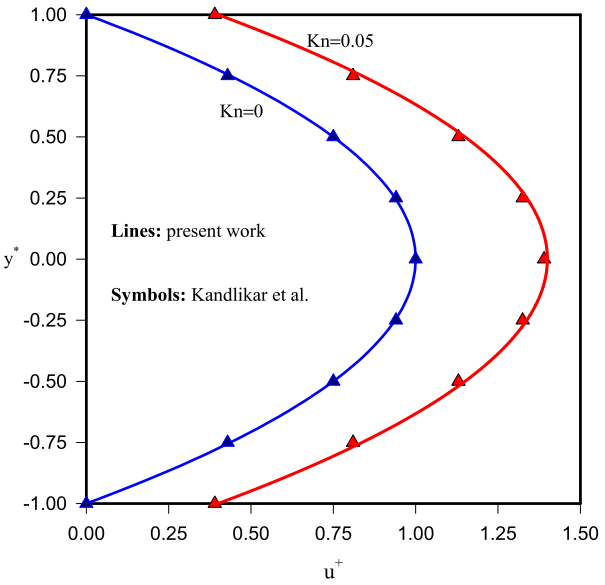

Fig. 3. Fully developed velocity profiles from LBM against those of analytical solution by Kandlikar et al. [2] where $u^+ = u/((-h^2/2\mu)(dp/dx))$ and $y^* = y/h$.

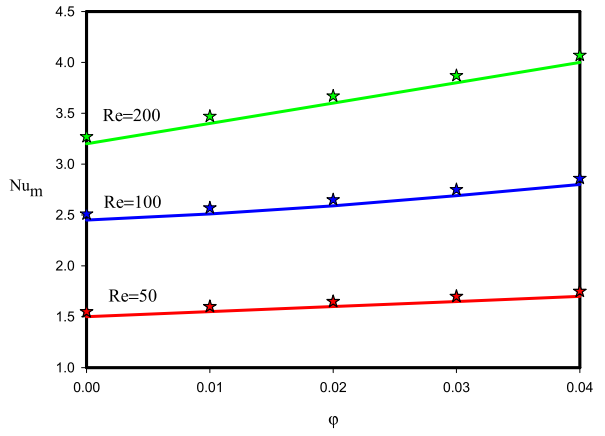

Fig. 4. Averaged Nusselt number versus Santra et al. [34] for the nanofluid simulation.

Suitable collision operator according to BGK [18]:

$$\Omega(f) = -\frac{f - f^e}{\tau_f} \tag{4}$$

$$\Omega(g) = -\frac{g - g^e}{\tau_g} - fZ = 0.5\,(\boldsymbol{c} - \boldsymbol{u})^2\,\Omega(f) - fZ \tag{5}$$

The last term in right hand side of Eq. (5) illustrates the heat dissipation:

$$fZ = f(\mathrm{c} - \boldsymbol{u}) \cdot [\partial_t \boldsymbol{u} + (\mathrm{c} \cdot \nabla)\boldsymbol{u}] \tag{6}$$

Now the modified distribution functions of $\widetilde{f}_i$ and $\widetilde{g}_i$ can be written by using τ_f and τ_g which show the hydrodynamic and thermal relaxation times,

$$\widetilde{f}_i = f_i + \frac{dt}{2\tau_f}(f_i - f_i^e) \tag{7}$$

$$\widetilde{g}_i = g_i + \frac{dt}{2\tau_g}(g_i - g_i^e) + \frac{dt}{2} f_i Z_i \tag{8}$$

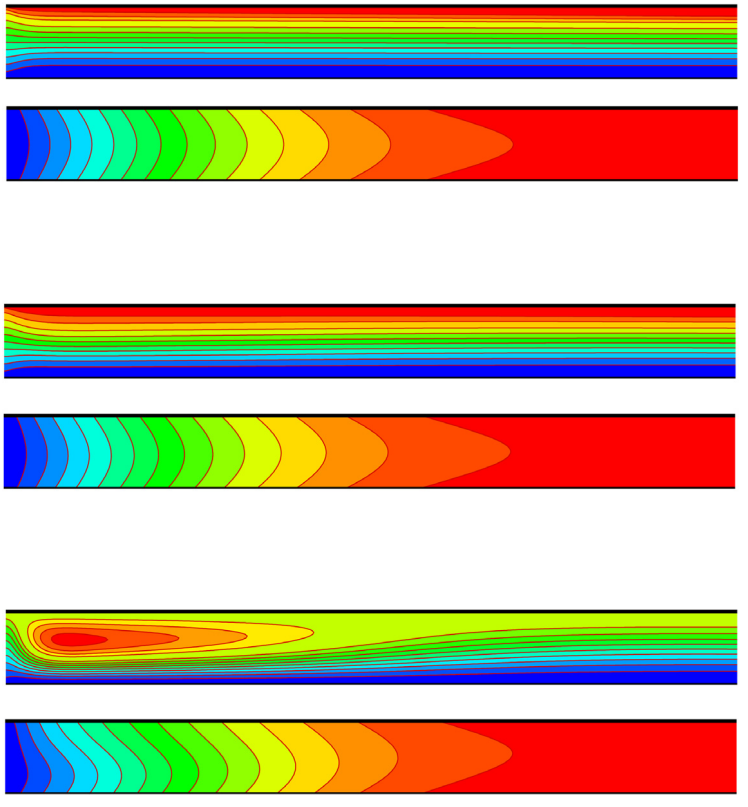

Fig. 5. Streamlines and isotherms at B = 0.005 and $\phi = 0.1\%$ for no-gravity (top), $Ri = 1$ (middle) and $Ri = 10$ (bottom).

f_i^e and g_i^e in Eqs. (7) and (8), represent the equilibrium distribution functions. Discretized microscopic velocity is achieved by using D_2Q_9 model (Fig. 2) which corresponds to a two dimensional geometry with 9 fictive nodes on each lattice,

$$Z_i = (\boldsymbol{c}_i - \boldsymbol{u}) \cdot D_i \boldsymbol{u} \qquad and \qquad D_i = \partial_t + \boldsymbol{c}_i \cdot \nabla \tag{9}$$

$$\begin{aligned} &\boldsymbol{c}_i = \left(\cos \tfrac{i-1}{2}\pi, \sin \tfrac{i-1}{2}\pi\right) \boldsymbol{c}, \quad i = 1, 2, 3, 4 \\ &\boldsymbol{c}_i = \sqrt{2}\left(\cos\left[\tfrac{(i-5)}{2}\pi + \tfrac{\pi}{4}\right], \sin\left[\tfrac{(i-5)}{2}\pi + \tfrac{\pi}{4}\right]\right) \boldsymbol{c}, \quad i = 5, 6, 7, 8 \\ &\boldsymbol{c}_0 = (0, 0) \end{aligned} \tag{10}$$

Collision and propagation at each time step of LBM are shown as follows,

$$\widetilde{f}_i(\boldsymbol{x} + \boldsymbol{c}_i dt, t + dt) - \widetilde{f}_i(\boldsymbol{x}, t) = -\frac{dt}{\tau_f + 0.5dt}\left[\widetilde{f}_i - f_i^e\right] \tag{11}$$

$$\widetilde{g}_i(\boldsymbol{x} + \boldsymbol{c}_i dt, t + dt) - \widetilde{g}_i(\boldsymbol{x}, t) = -\frac{dt}{\tau_g + 0.5dt}\left[\widetilde{g}_i - g_i^e\right] - \frac{\tau_g dt}{\tau_g + 0.5dt} f_i Z_i \tag{12}$$

$$f_i^e = \omega_i \rho \left[1 + \frac{3\boldsymbol{c}_i \cdot \boldsymbol{u}}{c^2} + \frac{9(\boldsymbol{c}_i \cdot \boldsymbol{u})^2}{2c^4} - \frac{3(u^2 + v^2)}{2c^2}\right] \tag{13}$$

$$\begin{aligned} &g_0^e = -\omega_0 \left[\tfrac{3\rho e}{2} \tfrac{u^2+v^2}{c^2}\right] \\ &g_{1,2,3,4}^e = \omega_1 \rho e \left[1.5 + 1.5\tfrac{\boldsymbol{c}_i \cdot \boldsymbol{u}}{c^2} + 4.5\tfrac{(\boldsymbol{c}_i \cdot \boldsymbol{u})^2}{c^4} - 1.5\tfrac{u^2+v^2}{c^2}\right] \\ &g_{5,6,7,8}^e = \omega_2 \rho e \left[3 + 6\tfrac{\boldsymbol{c}_i \cdot \boldsymbol{u}}{c^2} + 4.5\tfrac{(\boldsymbol{c}_i \cdot \boldsymbol{u})^2}{c^4} - 1.5\tfrac{u^2+v^2}{c^2}\right] \end{aligned} \tag{14}$$

$\rho e = \rho RT$ and the weigh functions are chosen as $\omega_0 = 4/9$, $\omega_i = 1/9$ for $i = 1, 2, 3, 4$ and $\omega_i = 1/36$ for $i = 5, 6, 7, 8$. Finally the macroscopic variables are derived from "f" and "g" as follows,

$$\begin{aligned} &\rho = \textstyle\sum_i \widetilde{f}_i \\ &\rho \boldsymbol{u} = \textstyle\sum_i \boldsymbol{c}_i \widetilde{f}_i \end{aligned} \tag{15}$$

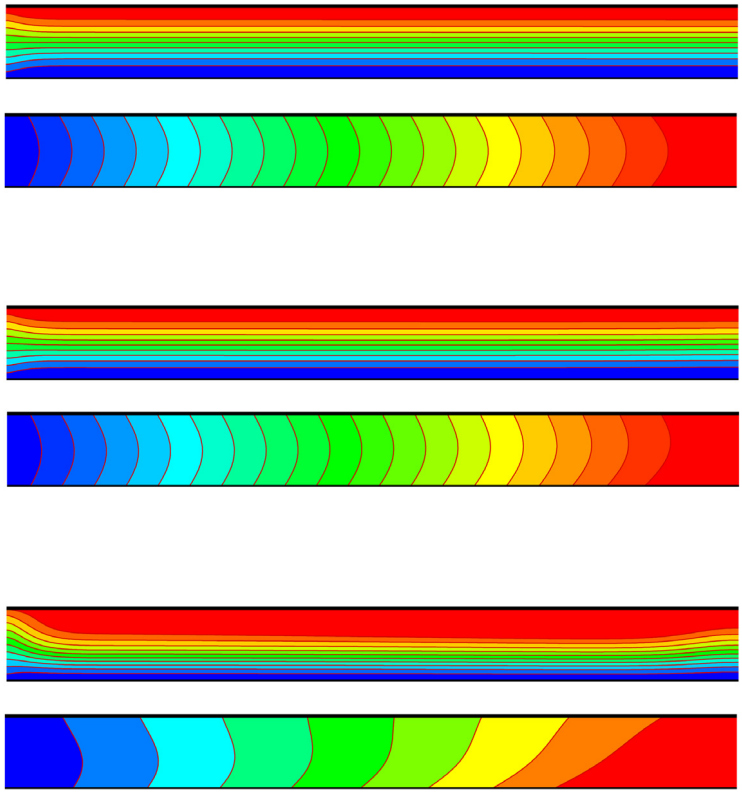

Fig. 6. Streamlines and isotherms at B = 0.02 and $\phi = 0.1\%$ for no-gravity (top), $Ri = 1$ (middle) and $Ri = 10$ (bottom).

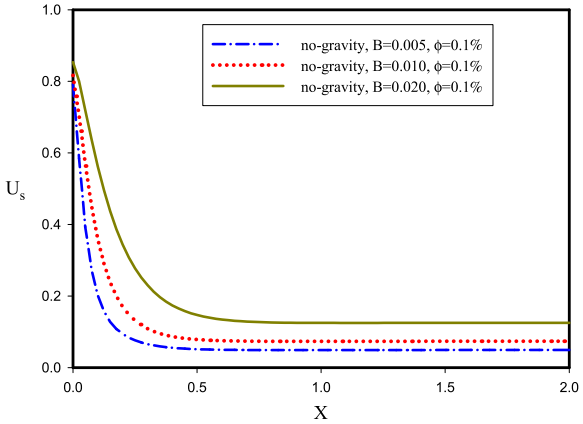

Fig. 7. The profiles of Slip velocity on the microchannel wall.

$$\rho e = \sum_i \widetilde{g}_i - \frac{dt}{2}\sum_i f_i Z_i \tag{16}$$

$$\tau_f = \sqrt{\frac{6}{\pi k}} D_H \cdot B \tag{17}$$

$$\tau_g = \frac{\tau_f}{\mathrm{Pr}} \tag{18}$$

3.2. Boundary conditions

Unknown hydrodynamic inlet and outlet distribution functions are determined by using the non-equilibrium bounce back model as follows,

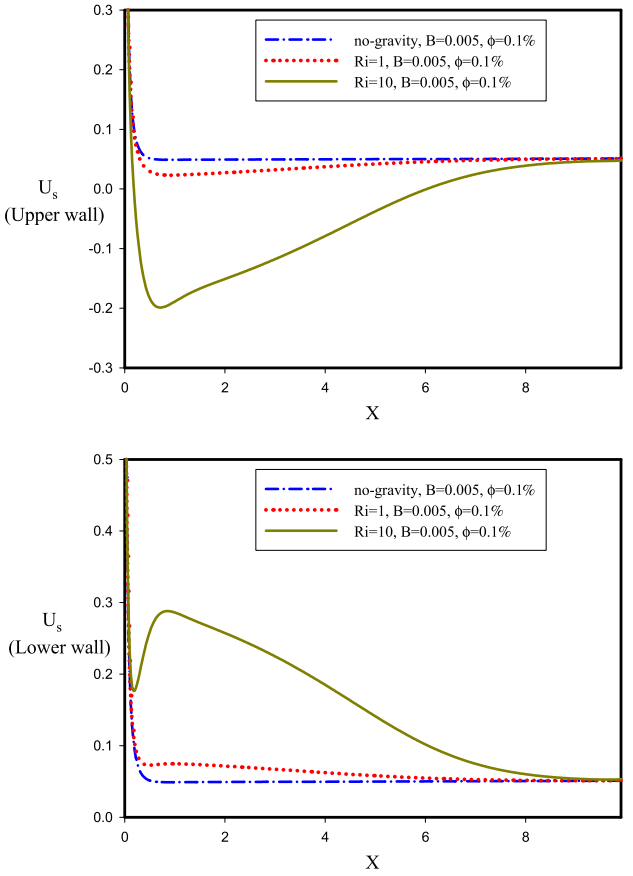

Fig. 8. U_s along the microchannel walls at B = 0.005.

$$
\begin{aligned}
\widetilde{f}_1 &= \widetilde{f}_3 + \tfrac{2}{3}\rho_{in}u_{in}\\
\widetilde{f}_5 &= \widetilde{f}_7 + \tfrac{1}{2}(\widetilde{f}_4 - \widetilde{f}_2) + \tfrac{1}{6}\rho_{in}u_{in}\\
\widetilde{f}_8 &= \widetilde{f}_6 - \tfrac{1}{2}(\widetilde{f}_4 - \widetilde{f}_2) + \tfrac{1}{6}\rho_{in}u_{in}
\end{aligned}
\tag{19}
$$

$$
\begin{aligned}
\widetilde{f}_3 &= \widetilde{f}_1 - \tfrac{2}{3}\rho_{out}u_{out}\\
\widetilde{f}_7 &= \widetilde{f}_5 - \tfrac{1}{2}(\widetilde{f}_4 - \widetilde{f}_2) - \tfrac{1}{6}\rho_{out}u_{out} - \tfrac{1}{2}\rho_{out}v_{out}\\
\widetilde{f}_6 &= \widetilde{f}_8 + \tfrac{1}{2}(\widetilde{f}_4 - \widetilde{f}_2) - \tfrac{1}{6}\rho_{out}u_{out} + \tfrac{1}{2}\rho_{out}v_{out}
\end{aligned}
\tag{20}
$$

Also for the unknown thermal inlet and outlet distribution functions as below [19–21]:

$$
\begin{aligned}
\widetilde{g}_5 &= \frac{6\rho e+3dt\sum_i f_i Z_i - 6(\widetilde{g}_0+\widetilde{g}_2+\widetilde{g}_3+\widetilde{g}_4+\widetilde{g}_6+\widetilde{g}_7)}{2+3u_{in}+3u_{in}^2}\times[3.0+6u_{in}+3.0u_{in}^2]\tfrac{1}{36}\\
\widetilde{g}_1 &= \frac{6\rho e+3dt\sum_i f_i Z_i - 6(\widetilde{g}_0+\widetilde{g}_2+\widetilde{g}_3+\widetilde{g}_4+\widetilde{g}_6+\widetilde{g}_7)}{2+3u_{in}+3u_{in}^2}\times[1.5+1.5u_{in}+3.0u_{in}^2]\tfrac{1}{9}\\
\widetilde{g}_8 &= \frac{6\rho e+3dt\sum_i f_i Z_i - 6(\widetilde{g}_0+\widetilde{g}_2+\widetilde{g}_3+\widetilde{g}_4+\widetilde{g}_6+\widetilde{g}_7)}{2+3u_{in}+3u_{in}^2}\times[3.0+6u_{in}+3.0u_{in}^2]\tfrac{1}{36}
\end{aligned}
\tag{21}
$$

$$
\begin{aligned}
\widetilde{g}_6 &= \frac{6(\widetilde{g}_1+\widetilde{g}_5+\widetilde{g}_8)-3dt\sum_i(\frac{c_{ix}}{c})Z_i f_i - 6\rho e u_{out}}{2-3u_{out}+3u_{out}^2}\times\\
&[3.0-6.0u_{out}+6.0v_{out}+3.0u_{out}^2+3.0v_{out}^2-9.0u_{out}v_{out}]\tfrac{1}{36}\\
\widetilde{g}_3 &= \frac{6(\widetilde{g}_1+\widetilde{g}_5+\widetilde{g}_8)-3dt\sum_i(\frac{c_{ix}}{c})Z_i f_i - 6\rho e u_{out}}{2-3u_{out}+3u_{out}^2}\times\\
&[1.5-1.5u_{out}+3.0u_{out}^2-1.50v_{out}^2]\tfrac{1}{9}\\
\widetilde{g}_7 &= \frac{6(\widetilde{g}_1+\widetilde{g}_5+\widetilde{g}_8)-3dt\sum_i(\frac{c_{ix}}{c})Z_i f_i - 6\rho e u_{out}}{2-3u_{out}+3u_{out}^2}\times\\
&[3.0-6.0u_{out}-6.0v_{out}+3.0u_{out}^2+3.0v_{out}^2+9.0u_{out}v_{out}]\tfrac{1}{36}
\end{aligned}
\tag{22}
$$

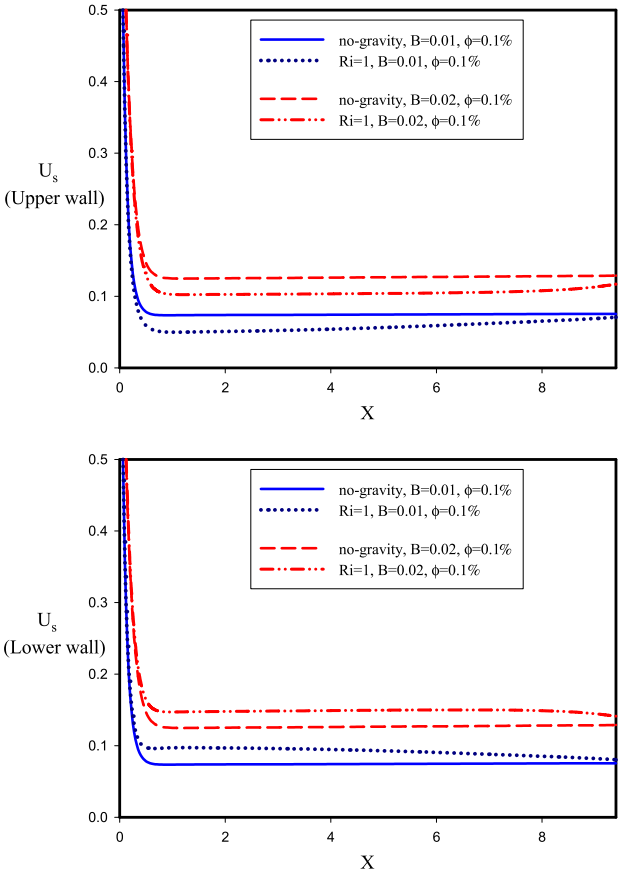

Fig. 9. U_s along the microchannel walls at B = 0.01 and B = 0.02.

Unknown hydrodynamic distribution functions along the lower wall of microchannel to simulate the slip velocity:

$$\widetilde{f}_2 = \widetilde{f}_4 \tag{23a}$$

$$\widetilde{f}_{5,6} = r\widetilde{f}_{7,8} + (1-r)\widetilde{f}_{8,7} \tag{23b}$$

where $r = 0.65$ represents the accommodation factor. Through the same procedure, the unknown hydrodynamic distribution functions along the upper wall of the microchannel:

$$\widetilde{f}_4 = \widetilde{f}_2 \tag{24a}$$

$$\widetilde{f}_{7,8} = r\widetilde{f}_{5,6} + (1-r)\widetilde{f}_{6,5} \tag{24b}$$

Eqs. (23) and (24) are able to simulate the slip velocity along the microchannel walls; however the effects of slip coefficient would be involved in Eq. (17).

3.3. Effects of gravity

Nanofluid mixed convection in a microchannel is investigated using Boussinesq approximation and based on the buoyancy force of $\mathbf{G} = \beta\mathbf{g}(\mathrm{T} - \overline{\mathrm{T}})$. Hence Boltzmann equation included the external force of "F" is achieved [8]:

$$\partial_t f + (\boldsymbol{c}\cdot\nabla)f = -\frac{f - f^e}{\tau_f} + F \tag{25}$$

"F" according to the buoyancy force is presented as $\mathrm{F} = \frac{\mathbf{G}.(\mathbf{c}-\mathbf{u})}{\mathrm{RT}}\mathrm{f}^{\mathrm{e}}$,

$$\begin{aligned} &f(\boldsymbol{x}+\boldsymbol{c}dt, \boldsymbol{c}, t+dt) - f(\boldsymbol{x}, \boldsymbol{c}, t) = -\tfrac{dt}{2\tau_f}\left[f(\boldsymbol{x}+\boldsymbol{c}dt, \boldsymbol{c}, t+dt) - f^e(\boldsymbol{x}+\boldsymbol{c}dt, \boldsymbol{c}, t+dt)\right] \\ &-\tfrac{dt}{2\tau_f}\left[f(\boldsymbol{x}, \boldsymbol{c}, t) - f^e(\boldsymbol{x}, \boldsymbol{c}, t)\right] + \tfrac{dt}{2}F(\boldsymbol{x}+\boldsymbol{c}dt, \boldsymbol{c}, t+dt) + \tfrac{dt}{2}F(\boldsymbol{x}, \boldsymbol{c}, t) \end{aligned} \tag{26}$$

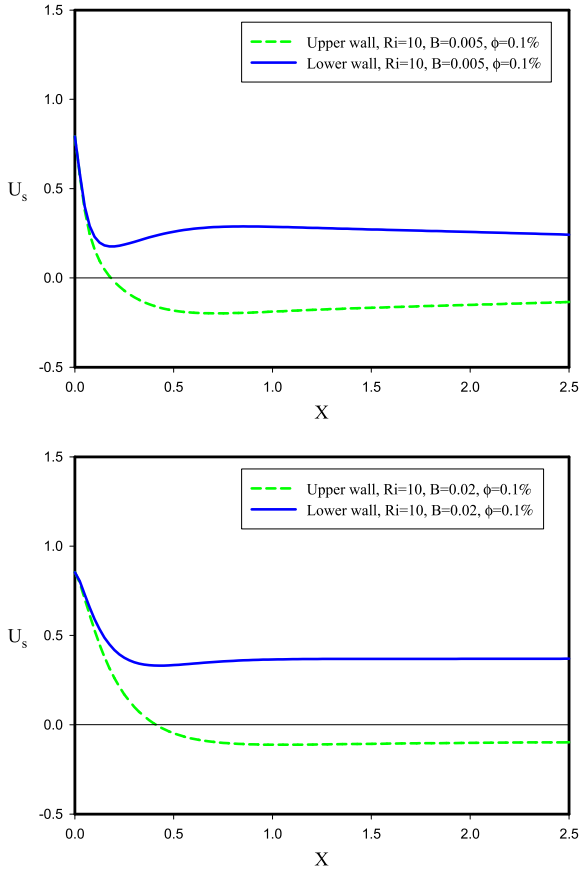

Fig. 10. U_s along the microchannel walls at $Ri = 10$.

$$\widetilde{f}(\boldsymbol{x}+\boldsymbol{c}dt,\boldsymbol{c},t+dt)-\widetilde{f}(\boldsymbol{x},\boldsymbol{c},t)=-\frac{dt}{\tau_f+0.5dt}\left[\widetilde{f}(\boldsymbol{x},\boldsymbol{c},t)-f^e(\boldsymbol{x},\boldsymbol{c},t)\right]+\frac{\tau_f F dt}{\tau_f+0.5dt} \tag{27}$$

Using equation of $\widetilde{f}_i = f_i + 0.5dt/\tau_f(f_i - f_i^e) - 0.5dtF$ leads to discretized form of Eq. (27):

$$\widetilde{f}_i(\boldsymbol{x}+\boldsymbol{c}_i dt,t+dt)-\widetilde{f}_i(\boldsymbol{x},t)=-\frac{dt}{\tau_f+0.5dt}\left[\widetilde{f}_i-f_i^e\right]+\left(\frac{dt\,\tau_f}{\tau_f+0.5dt}\frac{3G(c_{iy}-v)}{c^2}f_i^e\right) \tag{28}$$

$$f_i=\frac{\tau_f\widetilde{f}_i+0.5dtf_i^e}{\tau_f+0.5dt}+\left(\frac{0.5dt\,\tau_f}{\tau_f+0.5dt}\frac{3G(c_{iy}-v)}{c^2}f_i^e\right) \tag{29}$$

As a result and for the macroscopic variables with considering gravity:

$$\rho=\sum_i\widetilde{f}_i \tag{30a}$$

$$u=(1/\rho)\sum_i\widetilde{f}_i c_{ix} \tag{30b}$$

$$v=(1/\rho)\sum_i\widetilde{f}_i c_{iy}+\frac{dt}{2}G \tag{30c}$$

For the hydrodynamic boundary conditions at inlet while including buoyancy forces:

$$\widetilde{f}_1+\widetilde{f}_5+\widetilde{f}_8=\rho_{in}-(\widetilde{f}_0+\widetilde{f}_2+\widetilde{f}_3+\widetilde{f}_4+\widetilde{f}_6+\widetilde{f}_7) \tag{31a}$$

$$\widetilde{f}_1+\widetilde{f}_5+\widetilde{f}_8=\rho_{in}u_{in}+(\widetilde{f}_3+\widetilde{f}_6+\widetilde{f}_7) \tag{31b}$$

$$\widetilde{f}_5-\widetilde{f}_8=\rho_{in}v_{in}+(-\widetilde{f}_2+\widetilde{f}_4-\widetilde{f}_6+\widetilde{f}_7)-\frac{dt}{2}\rho_{in}G \tag{31c}$$

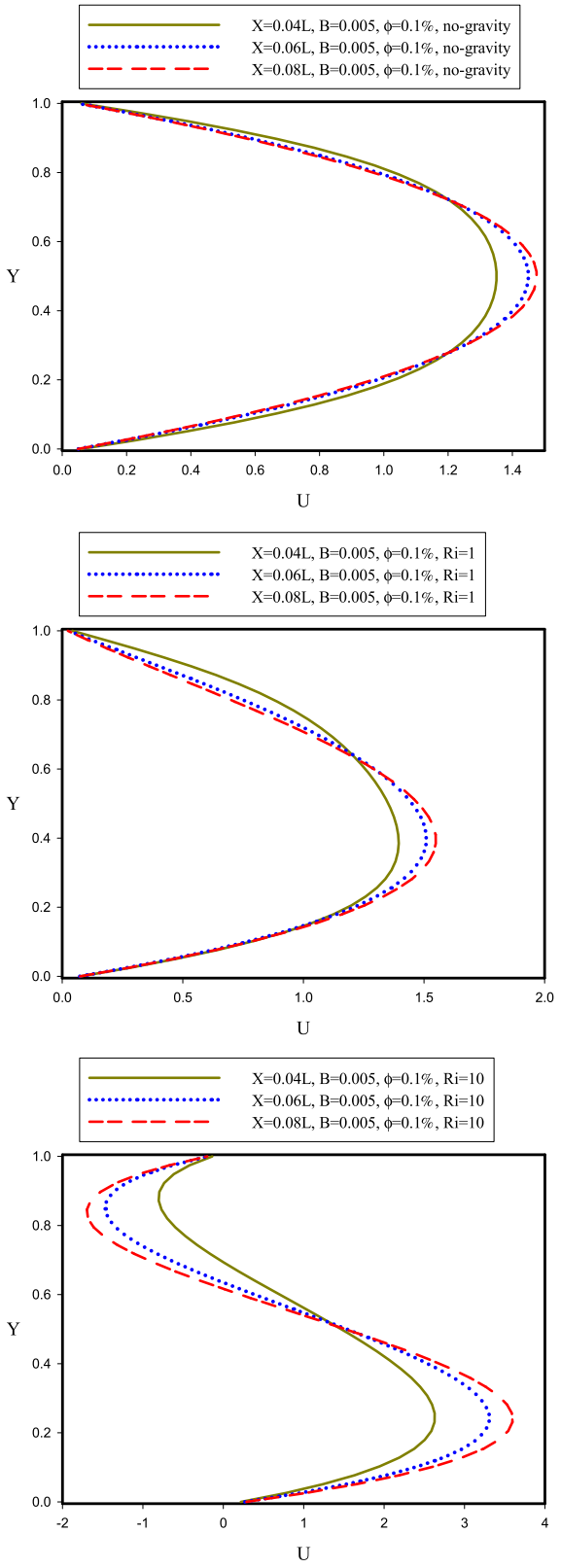

Fig. 11. The profiles of U at different vertical cross sections of the microchannel.

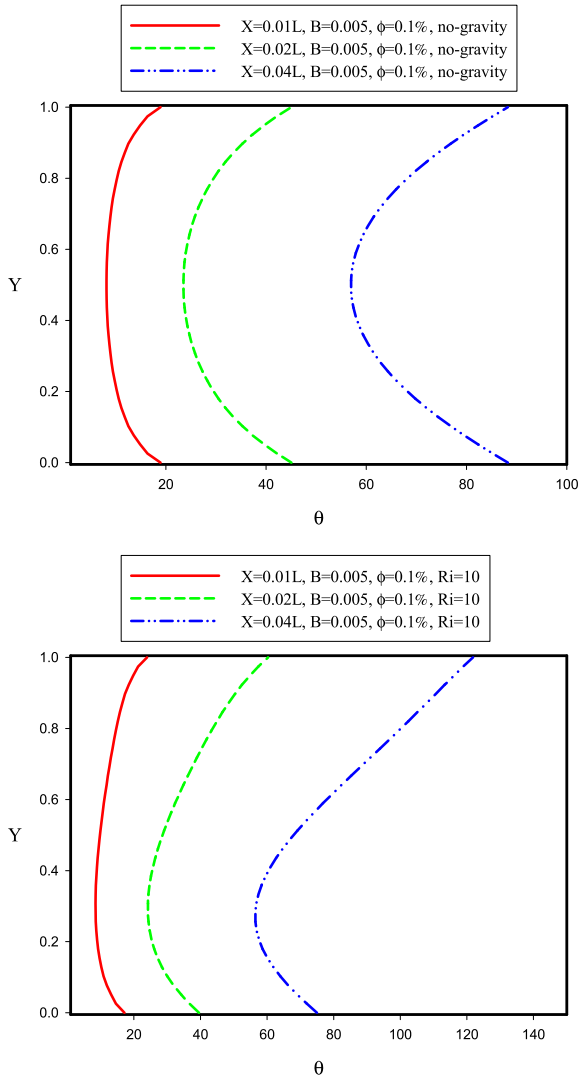

Fig. 12. The profiles of dimensionless temperature at different vertical cross sections.

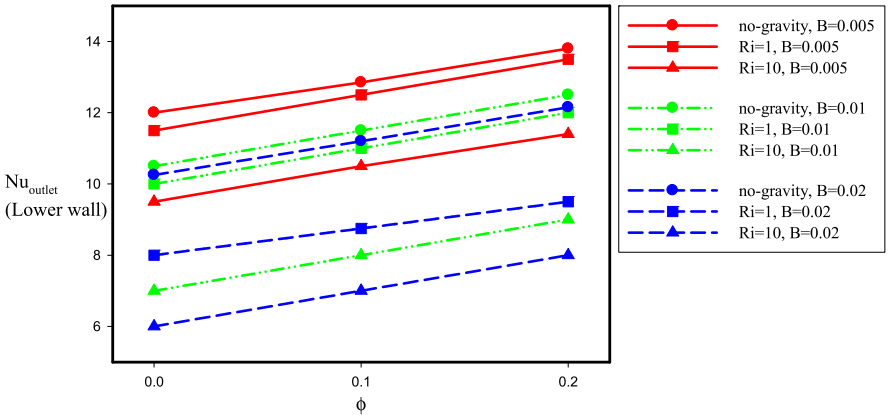

Fig. 13. Outlet Nusselt number on the lower wall of microchannel at different values of Ri, B and percent of ϕ.

where

$$\rho_{in} = \frac{\widetilde{f}_0 + \widetilde{f}_2 + \widetilde{f}_4 + 2(\widetilde{f}_3 + \widetilde{f}_6 + \widetilde{f}_7)}{1 - u_{in}} \tag{32}$$

and

$$\widetilde{f}_1 - \widetilde{f}_1^e = \widetilde{f}_3 - \widetilde{f}_3^e \Rightarrow \widetilde{f}_1 = \widetilde{f}_3 - \widetilde{f}_3^e + \widetilde{f}_1^e \tag{33}$$

From Eq. (13) beside Eqs. (31b), (31c) and (34) leads to:

$$\widetilde{f}_1 = \widetilde{f}_3 + \frac{2}{3}\rho_{in}u_{in} \tag{34}$$

$$\begin{aligned}\widetilde{f}_8 &= \widetilde{f}_6 - \frac{\widetilde{f}_4 - \widetilde{f}_2}{2} + \frac{1}{6}\rho_{in}u_w - \frac{1}{2}\rho_{in}v_{in} + \frac{dt}{4}\rho_{in}G\\ \widetilde{f}_5 &= \widetilde{f}_7 + \frac{\widetilde{f}_4 - \widetilde{f}_2}{2} + \frac{1}{6}\rho_{in}u_{in} + \frac{1}{2}\rho_{in}v_{in} - \frac{dt}{4}\rho_{in}G\end{aligned} \tag{35}$$

Similarly for outlet and considering buoyance forces:

$$\begin{aligned}\widetilde{f}_3 &= \widetilde{f}_1 - \tfrac{2}{3}\rho_{out}u_{out}\\ \widetilde{f}_7 &= \widetilde{f}_5 - \tfrac{1}{2}(\widetilde{f}_4 - \widetilde{f}_2) - \tfrac{1}{6}\rho_{out}u_{out} - \tfrac{1}{2}\rho_{out}v_{out} + \tfrac{1}{4}dt\rho_{out}G\\ \widetilde{f}_6 &= \widetilde{f}_8 + \tfrac{1}{2}(\widetilde{f}_4 - \widetilde{f}_2) - \tfrac{1}{6}\rho_{out}u_{out} + \tfrac{1}{2}\rho_{out}v_{out} - \tfrac{1}{4}dt\rho_{out}G\end{aligned} \tag{36}$$

Now it should be mentioned that slip velocity involving "G" is presented as below [8],

$$\widetilde{f}_2 + \widetilde{f}_5 + \widetilde{f}_6 = \rho_w v_w + (\widetilde{f}_4 + \widetilde{f}_7 + \widetilde{f}_8) - \frac{dt}{2}\rho_w G \tag{37}$$

$$\begin{aligned}\widetilde{f}_2 &= \widetilde{f}_4 - \tfrac{1}{2}dt\rho G\\ \widetilde{f}_5 &= r\widetilde{f}_7 + (1-r)\widetilde{f}_8\\ \widetilde{f}_6 &= r\widetilde{f}_8 + (1-r)\widetilde{f}_7\end{aligned} \tag{38}$$

As it was said before, the lower and upper walls were affected by a constant heat flux as follows [17],

$$\boldsymbol{q} = \left(\sum_i \boldsymbol{c}_i\widetilde{g}_i - \rho e\boldsymbol{u} - \frac{dt}{2}\sum_i \boldsymbol{c}_i f_i Z_i\right)\frac{\tau_g}{\tau_g + 0.5dt} \tag{39}$$

Using the last equation for the upper wall leads to:

$$\sum_i \boldsymbol{c}_{iy}\widetilde{g}_i = 0.5dt\sum_i \boldsymbol{c}_{iy}f_i Z_i + \rho e_N V_w + \frac{\tau_g + 0.5dt}{\tau_g}q_y \tag{40}$$

At last the following model is demonstrated considering the heat flux boundary condition in LBM form:

$$\begin{aligned}\widetilde{g}_4 &= \left[\frac{1}{\frac{1}{3} - \frac{1}{2}\frac{V_w}{c} + \frac{1}{2}\frac{V_w{}^2}{c^2}}\right]\times\\ &\left[(\widetilde{g}_2 + \widetilde{g}_5 + \widetilde{g}_6) - \tfrac{dt}{2}\textstyle\sum_{i=1}^{8}\frac{c_{iy}}{c}Z_i f_i - \rho e_N\frac{V_w}{c} - \frac{\tau_g + 0.5dt}{\tau_g}\frac{q_y}{c}\right]\times\\ &\omega_4\left[1.5 + 1.5\frac{\boldsymbol{c}_4\cdot\boldsymbol{u}_w}{c^2} + 4.5\frac{(\boldsymbol{c}_4\cdot\boldsymbol{u}_w)^2}{c^4} - 1.5\frac{U_w^2 + V_w{}^2}{c^2}\right]\end{aligned} \tag{41}$$

$$\begin{aligned}\widetilde{g}_{7,8} &= \left[\frac{1}{\frac{1}{3} - \frac{1}{2}\frac{V_w}{c} + \frac{1}{2}\frac{V_w{}^2}{c^2}}\right]\times\\ &\left[(\widetilde{g}_2 + \widetilde{g}_5 + \widetilde{g}_6) - \tfrac{dt}{2}\textstyle\sum_{i=1}^{8}\frac{c_{iy}}{c}Z_i f_i - \rho e_N\frac{V_w}{c} - \frac{\tau_g + 0.5dt}{\tau_g}\frac{q_y}{c}\right]\times\\ &\omega_{7,8}\left[3 + 6\frac{\boldsymbol{c}_{7,8}\cdot\boldsymbol{u}_w}{c^2} + 4.5\frac{(\boldsymbol{c}_{7,8}\cdot\boldsymbol{u}_w)^2}{c^4} - 1.5\frac{U_w^2 + V_w{}^2}{c^2}\right]\end{aligned} \tag{42}$$

Eqs. (41) and (42) are presented according to GPTBC model which are the developed forms of Dorazio et al. heat flux model [17]. Nusselt number equation based on the constant heat flux is written as:

$$Nu_x = \frac{q_y D_H}{\Delta T k} = \frac{D_H\,(\partial T/\partial y)_w}{T_w - T_{balk}} \tag{43}$$

Table 1
Grid independency study for the slip velocity at the state of no-gravity and $\phi = 0.1\%$.

	Mesh		
	350×35	400×40	450×45
$B = 0.02$	0.124	0.125	0.125
$B = 0.01$	0.072	0.073	0.073

Table 2
Thermo-physical properties of the FMWCNT/water nanofluid at different values of nanoparticles mass fraction [32].

ϕ % FMWCNT/water	ρ (Kg/m^3)	K (W/mK)	μ (Pas)
Pure water	996	0.62	7.65×10^{-4}
Pure water + 0.1% of FMWCNT	1003	0.66	7.81×10^{-4}
Pure water + 0.2% of FMWCNT	1006	0.71	7.90×10^{-4}

4. Grid independence study and validation

Three various nodes of 350×35, 400×40 and 450×45 were used in order to grid independency study and ignorable differences were found between those of 400×40 and 450×45; so that the lattice grids of 400×40 were selected for further computations (see Table 1). Present work achievements by LBM versus analytical ones of Kandlikar et al. [2] are compared in Fig. 3 corresponded to a plane flow between two parallel plates at width of 2h. The slip velocity is involved analytically as $u^+ = 1-y^{*2} + 8Kn$ in Ref. [2] where $u^+ = u/((-h^2/2\mu)(dp/dx))$ and $y^* = y/h$. Suitable agreements are seen between them. Moreover the averaged Nusselt number values of water/Cu nanofluid flow and heat transfer through a hot wall channel are compared with those of Santra et al. [34] in Fig. 4 and desirable accuracies are also observed in this figure.

5. Results

Nanofluid mixed convection in a microchannel is studied numerically by lattice Boltzmann method. Water as the base fluid and FMWCNT as the nanoparticles are selected in a homogeneous condition (see Table 2). Microchannel side walls are affected by a heat flux of q''_0. The temperature of inlet cold nanofluid increases through the microchannel due to heat exchange with the hot walls. Effects of gravity on slip velocity and temperature domain at different values of mass fraction as $\phi = 0$, $\phi = 0.1\%$ and $\phi = 0.2\%$ are investigated for three different cases of no-gravity, $Ri = 1$ and $Ri = 10$ at $Re = 1$. Dimensionless slip coefficient changes from $B = 0.005$ to $B = 0.01$ and $B = 0.02$.

Fig. 5 shows the streamlines and isotherms at $B = 0.005$ and $\phi = 0.1\%$ for no-gravity, $Ri = 1$ and $Ri = 10$. The smooth horizontal streamlines from the inlet left side and their corresponded symmetry isotherms due to the incoming heat flux from the lower and upper walls, are well obvious for the case of no-gravity. However these trends are vanished at higher amounts of Ri so that a strong long cell is generated at entrance region because of severe buoyancy forces at this area for $Ri = 10$; moreover the symmetry forms of isotherms are lost at this case. The influences of more values of slip coefficient on streamlines and isotherms are shown in Fig. 6 which is related to $B = 0.02$ and $\phi = 0.1\%$. There is no cell in this figure at $Ri = 10$; however a noticeable downward flows are observed along the microchannel due to gravity effects. As a result, the buoyancy forces at higher Ri, will be more important at lower values of slip coefficient.

The profiles of dimensionless slip velocity along the microchannel walls are presented in Fig. 7 for the state of no-gravity which implies the absence of gravity effects. The largest amount of slip velocity is occurred at inlet while it will decrease mildly with X to approach a constant value. Obviously, more B corresponds to more U_s. The effects of higher Ri on U_s are presented in Fig. 8 corresponded to $B = 0.005$. A strong downward variation in U_s is observed along the upper wall at $Ri = 10$, then mildly upward variation through it to reach its corresponded constant value. An interesting fact: generate a negative slip velocity in the region of $0.2 < X < 6$ along the upper wall and also observe a fluctuation in U_s along the lower wall which are the results of the rotational cell (observed in previous figure). In the following, the effects of different amounts of slip coefficient on slip velocity at various Richardson numbers are shown in Fig. 9 along the two horizontal microchannel walls. Fig. 10 illustrates U_s profiles along the microchannel walls at $Ri = 10$ for $B = 0.005$ and $B = 0.02$. Negative slip velocity along the upper wall can also be seen in this figure which implies the fluid flow in opposite direction of X due to existence the rotational cell. The effects of gravity along the lower wall are sensed by some fluctuations on U_s profiles through it.

Fig. 11 shows the profiles of U at different vertical cross sections of the microchannel for $B = 0.005$ at different Ri. The parabolic symmetric profiles of U and also a little amount of slip velocity at $Y = 0$ and $Y = 1$ are observed at no-gravity state which leads to have velocity a little less than 1.5 at $Y = 0.5$. Downward horizontal dimensionless velocity profiles, $U = u/u_i$, obviously can be seen in the plots corresponded to $Ri = 1$ which represent the influences of buoyancy forces; until that at $0.5 < Y < 1$ for $Ri = 10$, the profiles of U are negative and their amplitude would increase with X.

The profiles of dimensionless temperature of $\theta = T/T_i$ at different vertical cross sections at the case of no-gravity and $Ri = 10$ are presented in Fig. 12 for $B = 0.005$. The increase of nanofluid temperature affected by imposed heat flux from the horizontal walls and also the significant effects of buoyancy forces on the thermal domain are completely obvious in this

figure so that the symmetry forms of θ profiles in no-gravity state, would be vanished at $Ri = 10$ plots. Eventually the local Nusselt number values at the outlet of the microchannel lower wall (Nu_{outlet}) for different amounts of Ri, B and percent of ϕ are presented in Fig. 13. Higher mass fraction of FMWCNT corresponds to higher Nu; while more amounts of Nu are achieved at lower Ri. Moreover it is seen that larger slip coefficient leads to less outlet Nusselt number. However in the absence of buoyancy forces, the most value of Nu is achieved at $B = 0.005$.

Hence it is worth to say that the most heat transfer rate will be occurred at higher amounts of nanoparticles mass fraction and in the lower amounts of slip coefficient besides in the absence or ignorable amounts of buoyancy forces; which means the effects of gravity should be included at the small levels of the slip coefficient through the liquid micro flows.

6. Conclusion

Water/FMWCNT nanofluid mixed convection in a microchannel was studied numerically by lattice Boltzmann method; while the horizontal sidewalls were imposed by a constant heat flux. Double population distribution functions approach of LBM, had not been applied to simulate the effects of gravity on slip velocity and temperature domain of nanofluid in a micro flow. However present work improved the LBM performance in such mentioned cases for the first time.

Moreover the following points can be addressed in brief:

1- The smooth horizontal streamlines from the inlet left side and their corresponded symmetry isotherms due to the incoming heat flux from the lower and upper walls, are well obvious for the case of no-gravity. However these trends are vanished at higher amounts of Ri so that a strong long cell is generated at entrance region because of severe buoyancy forces at this area for $Ri = 10$; moreover the symmetry forms of isotherms are lost at this case. As a result, the buoyancy forces at higher Ri, will be more important at lower values of slip coefficient.

2- More slip coefficient corresponds to higher slip velocity. An interesting fact: generate a negative slip velocity (fluid flow in opposite direction of X) in the region of $0.2 < X < 6$ along the upper wall and also observe a fluctuation in slip velocity profile along the lower wall.

3- Higher mass fraction of FMWCNT corresponds to larger outlet Nusselt number; while more amounts of Nu are achieved at lower Ri. Moreover larger slip coefficient leads to less Nu. However in the absence of buoyancy forces, the most value of Nu is achieved at $B = 0.005$.

4- The most heat transfer rate will be occurred at higher amounts of nanoparticles mass fraction and in the lower amounts of slip coefficient besides in the absence or ignorable amounts of buoyancy forces; which means the effects of gravity should be included at the small levels of the slip coefficient through the liquid micro flows.

References

[1] N.T. Nguyen, S.T. Wereley, Fundamentals and Applications of Microfluidics, second ed., Artech house INC, Norwood, MA 02062, 2006.
[2] S. Kandlikar, S. Garimella, D. Li, S. Colin, M.R. King, Heat transfer and fluid flow in minichannels and microchannels, 2006.
[3] M. Gad-el Hak, Flow physics in MEMS, Rev. Mec. Ind. 2 (2001) 313–341.
[4] K. Hooman, A. Ejlali, Effects of viscous heating, fluid property variation, velocity slip, and temperature jump on convection through parallel plate and circular microchannels, Int. Commun. Heat Mass Transfer 37 (1) (2010) 34–38.
[5] H.P. Kavehpour, M. Faghri, Y. Asako, Effects of compressibility and rarefaction on gaseous flows in microchannels, Numer. Heat Transfer A 32 (1997) 677–696.
[6] M.R. Safaei, F. Omid Mahian, Garoosi, K. Hooman, Arash Karimipour, S.N. Kazi, S. Gharehkhani, Investigation of micro-and nanosized particle erosion in a 90 pipe bend using a two-phase discrete phase model, Sci. World J. 2014 (2014) 740578.
[7] Shamshirband Shahaboddin, Amir Malvandi, Arash Karimipour, Marjan Goodarzi, Masoud Afrand, Dalibor Petković, Mahidzal Dahari, Naghmeh Mahmoodian, Performance investigation of micro-and nano-sized particle erosion in a 90 elbow using an ANFIS model, Powder Technol. 284 (2015) 336–343.
[8] Karimipour Arash, Alireza Hossein Nezhad, Annunziata D'Orazio, Ebrahim Shirani, Investigation of the gravity effects on the mixed convection heat transfer in a microchannel using lattice Boltzmann method, Int. J. Therm. Sci. 54 (2012) 142–152.
[9] Karimipour Arash, Habibollah Alipour, Omid Ali Akbari, Davood Toghraie Semiromi, Mohammad Hemmat Esfe, Studying the effect of indentation on flow parameters and slow heat transfer of water-silver nano-fluid with varying volume fraction in a rectangular two-dimensional micro channel, Ind. J. Sci. Technol. 8 (15) (2015) 51707.
[10] F. Liu, W. Shi, F. Wu, A lattice Boltzmann model for the generalized Boussinesq equation, Appl. Math. Comput. 274 (2016) 331–342.
[11] Akbari Omid Ali, Davood Toghraie, Arash Karimipour, Impact of ribs on flow parameters and laminar heat transfer of water–aluminum oxide nanofluid with different nanoparticle volume fractions in a three-dimensional rectangular microchannel, Adv. Mech. Eng. 7 (11) (2015) 1687814015618155.
[12] Akbari Omid Ali, Davood Toghraie, Arash Karimipour, Numerical simulation of heat transfer and turbulent flow of water nanofluids copper oxide in rectangular microchannel with semi-attached rib, Adv. Mech. Eng. 8 (4) (2016) 1687814016641016.
[13] G. Bird, Molecular Gas Dynamics and the Direct Simulation of Gas Flows, Oxford University Press, 1994.
[14] E.S. Oran, C.K. Oh, B.Z. Cybyk, Direct simulation Mont Carlo: Recent advances and applications, Ann. Rev. Fluid Mech. 30 (1998) 403–441.
[15] Y.H. Qian, D. d'Humieres, P. Lallemand, Lattice BGK models for Navier–Stokes equation, Europhys. Lett. 17 (1992) 479–484.
[16] Goodarzi Marjan, M.R. Safaei, A. Karimipour, K. Hooman, M. Dahari, S.N. Kazi, E. Sadeghinezhad, Comparison of the finite volume and lattice Boltzmann methods for solving natural convection heat transfer problems inside cavities and enclosures, Abstr. Appl. Anal. 2014 (2014) 762184.
[17] D'Orazio Annunziata, Arash Karimipour, Alireza Hossein Nezhad, Ebrahim Shirani, Lattice Boltzmann method with heat flux boundary condition applied to mixed convection in inclined lid driven cavity, Meccanica 50 (4) (2015) 945–962.
[18] P.L. Bhatnagar, E.P. Gross, M. Krook, A model for collision process in gases. I. Small amplitude processes in charged and neutral one-component system, Phys. Rev. 94 (1954) 511–522.
[19] A. D'Orazio, M. Corcione, G.P. Celata, Application to natural convection enclosed flows of a lattice Boltzmann BGK model coupled with a general purpose thermal boundary condition, Int. J. Therm. Sci. 43 (2004) 575–586.
[20] A. D'Orazio, S. Succi, Simulating two-dimensional thermal channel flows by means of a lattice Boltzmann method with new boundary conditions, Future Gener. Comput. Syst. 20 (2004) 935–944.

[21] A. D'Orazio, S. Succi, C. Arrighetti, Lattice Boltzmann simulation of open flows with heat transfer, Phys. Fluids 15 (2003) 2778–2781.
[22] Y. Xuan, Q. Li, M. Ye, Investigations of convective heat transfer in ferrofluid microflows using lattice-Boltzmann approach, Int. J. Therm. Sci. 46 (2007) 105–111.
[23] Karimipour Arash, Alireza Hossein Nezhad, Annunziata D'Orazio, Ebrahim Shirani, The effects of inclination angle and Prandtl number on the mixed convection in the inclined lid driven cavity using lattice Boltzmann method, J. Theoret. Appl. Mech. 51 (2) (2013) 447–462.
[24] X. He, S. Chen, G.D. Doolen, A novel thermal model for the lattice Boltzmann method in incompressible limit, J. Comput. Phys. 146 (1998) 282–300.
[25] X. Nie, G.D. Doolen, S. Chen, Lattice-Boltzmann simulation of fluid flows in MEMS, J. Stat. Phys. 107 (2002) 279–289.
[26] S. Chen, G.D. Doolen, Lattice Boltzmann method for fluid flows, Annu. Rev. Fluid Mech. 30 (1998) 329–364.
[27] S. Chen, Z. Tian, Entropy generation analysis of thermal micro-Couette flows in slip regime, Int. J. Therm. Sci. 49 (2010) 2211–2221.
[28] S. Chen, Z. Tian, Simulation of thermal micro-flow using lattice Boltzmann method with Langmuir slip model, Int. J. Heat Fluid Flow 31 (2010) 227–235.
[29] Karimipour Arash, Mohammad Hemmat Esfe, Mohammad Reza Safaei, Davood Toghraie Semiromi, Saeed Jafari, S.N. Kazi, Mixed convection of copper–water nanofluid in a shallow inclined lid driven cavity using the lattice Boltzmann method, Physica A 402 (2014) 150–168.
[30] Karimipour Arash, Alireza Hossein Nezhad, Annunziata D'Orazio, Mohammad Hemmat Esfe, Mohammad Reza Safaei, Ebrahim Shirani, Simulation of copper–water nanofluid in a microchannel in slip flow regime using the lattice Boltzmann method, Eur. J. Mech. B Fluids 49 (2015) 89–99.
[31] Karimipour Arash, New correlation for Nusselt number of nanofluid with Ag/Al 2 O 3/Cu nanoparticles in a microchannel considering slip velocity and temperature jump by using lattice Boltzmann method, Int. J. Therm. Sci. 91 (2015) 146–156.
[32] A. Amrollahi, A.M. Rashidi, Convection heat transfer of functionalized MWNT in aqueous fluids in laminar and turbulent flow at the entrance region, Int. Commun. Heat Mass Transfer 37 (2010) 717–723.
[33] Nikkhah Zahra, Arash Karimipour, Mohammad Reza Safaei, Pezhman Forghani-Tehrani, Marjan Goodarzi, Mahidzal Dahari, Somchai Wongwises, Forced convective heat transfer of water/functionalized multi-walled carbon nanotube nanofluids in a microchannel with oscillating heat flux and slip boundary condition, Int. Commun. Heat Mass Transfer 68 (2015) 69–77.
[34] A.K. Santra, S. Sen, N. Chakraborty, Study of heat transfer due to laminar flow of copper–water nanofluid through two isothermally heated parallel plates, Int. J. Therm. Sci. 48 (2009) 391–400.
[35] Alipour Habibollah, Arash Karimipour, Mohammad Reza Safaei, Davood Toghraie Semiromi, Omid Ali Akbari, Influence of T-semi attached rib on turbulent flow and heat transfer parameters of a silver-water nanofluid with different volume fractions in a three-dimensional trapezoidal microchannel, Physica E 88 (2017) 60–76.
[36] Sajadifar Seyed Ali, Arash Karimipour, Davood Toghraie, Fluid flow and heat transfer of non-Newtonian nanofluid in a microtube considering slip velocity and temperature jump boundary conditions, Eur. J. Mech. B Fluids 61 (2017) 25–32.
[37] Akbari Omid Ali, et al., The effect of velocity and dimension of solid nanoparticles on heat transfer in non-Newtonian nanofluid, Physica E 86 (2017) 68–75.
[38] Esfe Mohammad Hemmat, Wei-Mon Yan, Mohammad Akbari, Arash Karimipour, Mohsen Hassani, Experimental study on thermal conductivity of DWCNT-ZnO/water-EG nanofluids, Int. Commun. Heat Mass Transfer 68 (2015) 248–251.
[39] Esfe Mohammad Hemmat, Ali Akbar Abbasian Arani, Arash Karimiopour, Seyed Sadegh Mirtalebi Esforjani, Numerical simulation of natural convection around an obstacle placed in an enclosure filled with different types of nanofluids, Heat Transfer Res. 45 (3) (2014) 279–292.
[40] A. Asadollahi, A. Esmaeeli, Simulation of condensation and liquid break-up on a micro-object with upper and lower movable walls using Lattice Boltzmann Method, Physica A 498 (2018) 33–49.
[41] M. Nemati, A.R.S.N. Abady, D. Toghraie, A. Karimipour, Numerical investigation of the pseudopotential lattice Boltzmann modeling of liquid–vapor for multi-phase flows, Physica A 489 (2018) 65–77.
[42] H. Otomo, B.M. Boghosian, F. Dubois, Two complementary lattice-Boltzmann-based analyses for nonlinear systems, Physica A 486 (2017) 1000–1011.
[43] W. Zhao, L. Wang, W.A. Yong, On a two-relaxation-time D2Q9 lattice Boltzmann model for the Navier–Stokes equations, Physica A 492 (2018) 1570–1580.
[44] D. Toghraie, M. Mokhtari, M. Afrand, Molecular dynamic simulation of copper and platinum nanoparticles Poiseuille flow in a nanochannels, Physica E 84 (2016) 152–161.
[45] M. Rezaei, A.R. Azimian, D. Toghraie, Molecular dynamics study of an electro-kinetic fluid transport in a charged nanochannel based on the role of the stern layer, Physica A 426 (2015) 25–34.
[46] M. Rezaei, A.R. Azimian, D.T. Semiromi, The surface charge density effect on the electro-osmotic flow in a nanochannel: a molecular dynamics study, Heat Mass Transf. 51 (5) (2015) 661–670.
[47] M. Tohidi, D. Toghraie, The effect of geometrical parameters, roughness and the number of nanoparticles on the self-diffusion coefficient in couette flow in a nanochannel by using of molecular dynamics simulation, Physica B 518 (2017) 20–32.
[48] M. Afrand, D. Toghraie, A. Karimipour, S. Wongwises, A numerical study of natural convection in a vertical annulus filled with gallium in the presence of magnetic field, J. Magn. Magn. Mater. 430 (2017) 22–28.
[49] H. Noorian, D. Toghraie, A.R. Azimian, Molecular dynamics simulation of poiseuille flow in a rough nano channel with checker surface roughnesses geometry, Heat Mass Transf. 50 (1) (2014) 105–113.
[50] D.T. Semiromi, A.R. Azimian, Nanoscale Poiseuille flow and effects of modified Lennard–Jones potential function, Heat Mass Transf. 46 (7) (2010) 791–801.
[51] D.T. Semiromi, A.R. Azimian, Molecular dynamics simulation of annular flow boiling with the modified Lennard-Jones potential function, Heat Mass Transf. 48 (1) (2012) 141–152.
[52] O.A. Akbari, D. Toghraie, A. Karimipour, M.R. Safaei, M. Goodarzi, H. Alipour, M. Dahari, Investigation of rib's height effect on heat transfer and flow parameters of laminar water–Al2O3 nanofluid in a rib-microchannel, Appl. Math. Comput. 290 (2016) 135–153.
[53] M. Afrand, A.A. Nadooshan, M. Hassani, H. Yarmand, M. Dahari, Predicting the viscosity of multi-walled carbon nanotubes/water nanofluid by developing an optimal artificial neural network based on experimental data, Int. Commun. Heat Mass Transfer 77 (2016) 49–53.
[54] M. Goodarzi, A.S. Kherbeet, M. Afrand, E. Sadeghinezhad, M. Mehrali, P. Zahedi, S. Wongwises, M. Dahari, Investigation of heat transfer performance and friction factor of a counter-flow double-pipe heat exchanger using nitrogen-doped, graphene-based nanofluids, Int. Commun. Heat Mass Transfer 76 (2016) 16–23.
[55] M. Vafaei, M. Afrand, N. Sina, R. Kalbasi, F. Sourani, H. Teimouri, Evaluation of thermal conductivity of MgO-MWCNTs/EG hybrid nanofluids based on experimental data by selecting optimal artificial neural networks, Physica E 85 (2017) 90–96.
[56] M. Afrand, S. Farahat, A.H. Nezhad, G.A. Sheikhzadeh, F. Sarhaddi, Numerical simulation of electrically conducting fluid flow and free convective heat transfer in an annulus on applying a magnetic field, Heat Transfer Res. 45 (8) (2014) 749–766.
[57] M. Afrand, D. Toghraie, B. Ruhani, Effects of temperature and nanoparticles concentration on rheological behavior of Fe3O4–Ag/EG hybrid nanofluid: an experimental study, Exp. Therm Fluid Sci. 77 (2016) 38–44.
[58] M. Afrand, Experimental study on thermal conductivity of ethylene glycol containing hybrid nano-additives and development of a new correlation, Appl. Therm. Eng. 110 (2017) 1111–1119.
[59] M. Mahmoodi, M.H. Esfe, M. Akbari, A. Karimipour, M. Afrand, Magneto-natural convection in square cavities with a source–sink pair on different walls, Int. J. Appl. Electromagn. Mech. 47 (1) (2015) 21–32.

[60] M. Bahrami, M. Akbari, A. Karimipour, M. Afrand, An experimental study on rheological behavior of hybrid nanofluids made of iron and copper oxide in a binary mixture of water and ethylene glycol: non-Newtonian behavior, Exp. Therm Fluid Sci. 79 (2016) 231–237.
[61] M. Zadkhast, D. Toghraie, A. Karimipour, Developing a new correlation to estimate the thermal conductivity of MWCNT-CuO/water hybrid nanofluid via an experimental investigation, J. Therm. Anal. Calorim. 129 (2) (2017) 859–867.
[62] M. Esfandiary, B. Mehmandoust, A. Karimipour, H.A. Pakravan, Natural convection of Al2O3–water nanofluid in an inclined enclosure with the effects of slip velocity mechanisms: Brownian motion and thermophoresis phenomenon, Int. J. Therm. Sci. 105 (2016) 137–158.
[63] M. Goodarzi, A. Amiri, M.S. Goodarzi, M.R. Safaei, A. Karimipour, E.M. Languri, M. Dahari, Investigation of heat transfer and pressure drop of a counter flow corrugated plate heat exchanger using MWCNT based nanofluids, Int. Commun. Heat Mass Transfer 66 (2015) 172–179.
[64] A.R. Shirneshan, M. Almassi, B. Ghobadian, G.H. Najafi, Investigating the effects of biodiesel from waste cooking oil and engine operating conditions on the diesel engine performance by response surface methodology, Iran. J. Sci. Technol. Trans. Mech. Eng. 38 (M2) (2014) 289–301.
[65] A. Karimipour, A.H. Nezhad, A. Behzadmehr, S. Alikhani, E. Abedini, Periodic mixed convection of a nanofluid in a cavity with top lid sinusoidal motion, Proc. Inst. Mech. Eng. C 225 (9) (2011) 2149–2160.
[66] M. Afrand, S. Rostami, M. Akbari, S. Wongwises, M.H. Esfe, A. Karimipour, Effect of induced electric field on magneto-natural convection in a vertical cylindrical annulus filled with liquid potassium, Int. J. Heat Mass Transfer 90 (2015) 418–426.
[67] N. Motamedifar, A. Shirneshan, An experimental study of emission characteristics from cylindrical furnace: Effects of using diesel-ethanol-biodiesel blends and air swirl, Fuel 221 (2018) 233–239.
[68] A. Shirneshan, A. Nedayali, Investigation of the effects of biodiesel-diesel fuel blends on the performance and emission characteristics of a diesel engine, J. Teknol. 78 (6) (2016) 169–177.
[69] A. Shirneshan, M. Almassi, B. Ghobadian, A.M. Borghei, G. Najafi, Response surface methodology (RSM) based optimization of biodiesel-diesel blends and investigation of their effects on diesel engine operating conditions and emission characteristics, Environ. Eng. Manage. J. (EEMJ) 15 (12) (2016) 2771–2780.
[70] M. Goodarzi, M.R. Safaei, K. Vafai, G. Ahmadi, M. Dahari, S.N. Kazi, N. Jomhari, Investigation of nanofluid mixed convection in a shallow cavity using a two-phase mixture model, Int. J. Therm. Sci. 75 (2014) 204–220.
[71] M.H. Esfe, A. Karimipour, W.M. Yan, M. Akbari, M.R. Safaei, M. Dahari, Experimental study on thermal conductivity of ethylene glycol based nanofluids containing Al2O3 nanoparticles, Int. J. Heat Mass Transfer 88 (2015) 728–734.
[72] H. Togun, G. Ahmadi, T. Abdulrazzaq, A.J. Shkarah, S.N. Kazi, A. Badarudin, M.R. Safaei, Thermal performance of nanofluid in ducts with double forward-facing steps, J. Taiwan Inst. Chem. Eng. 47 (2015) 28–42.
[73] F. Mianzarasvand, A. Shirneshan, M. Afrand, Effect of electrically heated catalytic converter on emission characteristic of a motorcycle engine in cold-start conditions: CFD simulation and kinetic study, Appl. Therm. Eng. 127 (2017) 453–464.
[74] M.J. Saheban Alahadi, A. Shirneshan, M. Kolahdoozan, Experimental investigation of the effect of grooves cut over the piston surface on the volumetric efficiency of a radial hydraulic piston pump, Int. J. Fluid Power 18 (3) (2017) 181–187.
[75] R. Ranjbarzadeh, A. Karimipour, M. Afrand, A.H.M. Isfahani, A. Shirneshan, Empirical analysis of heat transfer and friction factor of water/graphene oxide nanofluid flow in turbulent regime through an isothermal pipe, Appl. Therm. Eng. 126 (2017) 538–547.
[76] M.R. Safaei, M. Safdari Shadloo, M.S. Goodarzi, A. Hadjadj, H.R. Goshayeshi, M. Afrand, S.N. Kazi, A survey on experimental and numerical studies of convection heat transfer of nanofluids inside closed conduits, Adv. Mech. Eng. 8 (10) (2016) 1687814016673569.
[77] M. Goodarzi, M.R. Safaei, H.F. Oztop, A. Karimipour, E. Sadeghinezhad, M. Dahari, S.N. Kazi, N. Jomhari, Numerical study of entropy generation due to coupled laminar and turbulent mixed convection and thermal radiation in an enclosure filled with a semitransparent medium, Sci. World J. (2014) 761745.
[78] A. Shirneshan, B.H. Samani, B. Ghobadian, Optimization of biodiesel percentage in fuel mixture and engine operating conditions for diesel engine performance and emission characteristics by Artificial Bees Colony Algorithm, Fuel 184 (2016) 518–526.
[79] A. Nedayali, A. Shirneshan, Experimental study of the effects of biodiesel on the performance of a diesel power generator, Energy Environ. 27 (5) (2016) 553–565.
[80] M.R. Safaei, B. Rahmanian, M. Goodarzi, Numerical study of laminar mixed convection heat transfer of power-law non-Newtonian fluids in square enclosures by finite volume method, Int. J. Phys. Sci. 6 (33) (2011) 7456–7470.
[81] M. Afrand, K.N. Najafabadi, M. Akbari, Effects of temperature and solid volume fraction on viscosity of SiO2-MWCNTs/SAE40 hybrid nanofluid as a coolant and lubricant in heat engines, Appl. Therm. Eng. 102 (2016) 45–54.
[82] M.H. Esfe, S.S.M. Esforjani, M. Akbari, A. Karimiopour, Mixed-convection flow in a lid-driven square cavity filled with a nanofluid with variable properties: effect of the nanoparticle diameter and of the position of a hot obstacle, Heat Transfer Res. 45 (6) (2014) 563–578.
[83] M. Afrand, A. Karimipour, A.A. Nadooshan, M. Akbari, The variations of heat transfer and slip velocity of FMWNT-water nano-fluid along the micro-channel in the lack and presence of a magnetic field, Physica E 84 (2016) 474–481.
[84] M. Akbari, M. Afrand, A. Arshi, A. Karimipour, An experimental study on rheological behavior of ethylene glycol based nanofluid: Proposing a new correlation as a function of silica concentration and temperature, J. Molecular Liquids 233 (2017) 352–357.
[85] M.H. Esfe, S. Niazi, S.S.M. Esforjani, M. Akbari, Mixed convection flow and heat transfer in a ventilated inclined cavity containing hot obstacles subjected to a nanofluid, Heat Transfer Res. 45 (4) (2014) 309–338.
[86] O. Soltani, M. Akbari, Effects of temperature and particles concentration on the dynamic viscosity of MgO-MWCNT/ethylene glycol hybrid nanofluid: experimental study, Physica E 84 (2016) 564–570.
[87] M. Akbari, S. Saedodin, D. Toghraie, R. Shoja-Razavi, F. Kowsari, Experimental and numerical investigation of temperature distribution and melt pool geometry during pulsed laser welding of Ti6Al4V alloy, Opt. Laser Technol. 59 (2014) 52–59.
[88] M.H. Esfe, M. Akbari, A. Karimipour, M. Afrand, O. Mahian, S. Wongwises, Mixed-convection flow and heat transfer in an inclined cavity equipped to a hot obstacle using nanofluids considering temperature-dependent properties, Int. J. Heat Mass Transfer 85 (2015) 656–666.
[89] S.S. Harandi, A. Karimipour, M. Afrand, M. Akbari, A. D'Orazio, An experimental study on thermal conductivity of F-MWCNTs–Fe3O4/EG hybrid nanofluid: effects of temperature and concentration, Int. Commun. Heat Mass Transfer 76 (2016) 171–177.
[90] M.H. Esfe, A. Ghadi, S.M. Esforjania, M. Akbari, Combined convection in a lid-driven cavity with an inside obstacle subjected to Al2O3-water nanofluid: effect of solid volume fraction and nanofluid variable properties, Acta Phys. Polon. A 124 (4) (2013).
[91] H. Yarmand, S. Gharehkhani, S.N. Kazi, E. Sadeghinezhad, M.R. Safaei, Numerical investigation of heat transfer enhancement in a rectangular heated pipe for turbulent nanofluid, Sci. World J. 2014 (2014).
[92] M.R. Safaei, H.R. Goshayeshi, B.S. Razavi, M. Goodarzi, Numerical investigation of laminar and turbulent mixed convection in a shallow water-filled enclosure by various turbulence methods, Sci. Res. Essays 6 (22) (2011) 4826–4838.
[93] H. Yarmand, G. Ahmadi, S. Gharehkhani, S.N. Kazi, M.R. Safaei, M.S. Alehashem, A.B. Mahat, Entropy generation during turbulent flow of zirconia-water and other nanofluids in a square cross section tube with a constant heat flux, Entropy 16 (11) (2014) 6116–6132.
[94] A. Karimipour, A. Taghipour, A. Malvandi, Developing the laminar MHD forced convection flow of water/FMWNT carbon nanotubes in a microchannel imposed the uniform heat flux, J. Magn. Magn. Mater. 419 (2016) 420–428.
[95] A. Karimipour, A. D'Orazio, M.S. Shadloo, The effects of different nano particles of Al2O3 and Ag on the MHD nano fluid flow and heat transfer in a microchannel including slip velocity and temperature jump, Physica E 86 (2017) 146–153.

[96] F. Peñuñuri, J.A. Montoya, O. Carvente, Density profiles of granular gases studied by molecular dynamics and Brownian bridges, Physica A 492 (2018) 2103–2110.
[97] M. Keskin, M. Ertaş, Frequency-dependent dynamic magnetic properties of the Ising bilayer system consisting of spin-3/2 and spin-5/2 spins, Physica A 496 (2018) 79–89.
[98] G. Torres-García, D.P. Luis, G. Odriozola, J. López-Lemus, Ethane clathrates using different water–ethane models: Molecular dynamics, Physica A 491 (2018) 89–100.